

# Quantum Monte Carlo Study of an Extended Hubbard Model on a Two-Leg Ladder

Tomo MUNEHISA and Yasuko MUNEHISA

Faculty of Engineering, Yamanashi University  
Kofu, Yamanashi, 400

## ABSTRACT

An extended Hubbard model on a two-leg ladder is numerically studied by means of the quantum Monte Carlo techniques. The model we study has the nearest-neighbor interactions which are repulsive along chains and attractive for rungs. The plots of the doping parameter versus the chemical potential show two cliff-like regions and a large plateau region. Results on the charge susceptibility suggest it diverges in these cliff-like regions. These observations might imply a signal to the phase separation, which should be related to the effective attractive interactions along chains.

KEYWORDS: Hubbard model, ladder, Monte Carlo, phase separation, charge gap

## §1 Introduction

The experimental realizations of the ladder systems[1], which is considered as a useful bridge to clarify the relation between one-dimensional and two-dimensional systems, have given theorists exciting topics in the study of the strongly correlated electrons. Works on the quantum spin systems[2], to which the half-filled Hubbard system reduces in the limit of the strong repulsive Coulomb interactions, show a striking contrast between the ladders with even legs, for which the finite spin gaps exist, and the odd-legged ladders which, as well as the one-dimensional (chain) case, show no spin gaps. The  $t$ - $J$  model on ladders is another object to be studied[3] in order to understand the doped system with the strong on-site Coulomb repulsion. Although we have not come to a very definite conclusion yet, interesting features like the  $d$ -wave correlations are suggested. Furthermore some numerical studies for the Hubbard ladder model have been carried out[4], but the issue of the long-range order of the pair-pair correlation functions seems controversial.

Recently various extended Hubbard models are under study to find the effects of the longer range interactions between the electrons[5]. In this paper we report numerical results obtained by the quantum Monte Carlo techniques on an extended Hubbard model with the two-leg ladder, whose Hamiltonian includes the Coulomb-like nearest-neighbor interactions that are repulsive along chains and attractive for rungs, studied in the conditions that the system is doped by holes or by electrons and the on-site Coulomb repulsion lies in the intermediate region. It should be noted that, for the values of the model's parameters we use in the simulation, the double occupancy is abundant so that holes can emerge even when electrons are doped to the system. Our motivation to study this model is to investigate behaviors caused by double-occupancy-pairs or vacancy-pairs on rungs, where (and hereafter) we refer to the state of a vacant site, a site upon which no electrons are sitting, as vacancy.

We measure some thermodynamical quantities concerning to the number of particles of the system such as the doping parameter and the charge susceptibility as a function of the chemical potential. We observe that the plots of the doping parameter versus the chemical potential show *two unexpected cliff-like regions at finite dopings* in addition to a few plateau regions, which have been expected from the re-

sults for the standard Hubbard model on the chain or the square lattice systems[6]. The charge susceptibility measured in each of the cliff-like regions shows a large peak which seemingly diverges at the temperature consistent with zero to imply the possibility of the phase separation that has not been confirmed in the preceding studies of the Hubbard-like models.

In §2 we make a brief description on the model and method. The Monte Carlo results are in §3 together with the definitions of the quantities we measured. Finally §4 is devoted to discussions.

## §2 the Model

The Hamiltonian we study is

$$\begin{aligned} \mathcal{H} = & -t_c \sum_{\sigma} \sum_l \sum_{i=1}^{N_r-1} [c_{i,l,\sigma}^{\dagger} c_{i+1,l,\sigma} + h.c.] - t_r \sum_{\sigma} \sum_{i=1}^{N_r} [c_{i,a,\sigma}^{\dagger} c_{i,b,\sigma} + h.c.] \\ & + V_c \sum_{\sigma,\sigma'} \sum_l \sum_{i=1}^{N_r-1} n_{i,l,\sigma} n_{i+1,l,\sigma'} + V_r \sum_{\sigma,\sigma'} \sum_{i=1}^{N_r} n_{i,a,\sigma} n_{i,b,\sigma'} + U \sum_l \sum_{i=1}^{N_r} n_{i,l,\uparrow} n_{i,l,\downarrow} \end{aligned} \quad (1)$$

where  $c_{i,l,\sigma}$  denotes the annihilation operator for an electron with spin  $\sigma$  ( $\uparrow$  or  $\downarrow$ ) which is located on the  $i$ -th rung along the leg  $l$  ( $a$  or  $b$ ) of a ladder,  $N_r$  being the total number of rungs and  $n_{i,l,\sigma} \equiv c_{i,l,\sigma}^{\dagger} c_{i,l,\sigma}$ . We employ an open boundary condition to avoid the hoppings between the sites on the first rung and the sites on the  $N_r$ -th rung.

The partition function  $Z$  is given by

$$Z = \text{tr}\{e^{-\beta(\mathcal{H}-\mu\mathcal{N})}\}, \quad (2)$$

with the inverse temperature  $\beta$ , the chemical potential  $\mu$  and

$$\mathcal{N} \equiv \sum_{\sigma} \sum_l \sum_{i=1}^{N_r} n_{i,l,\sigma}, \quad (3)$$

which is the total number of electrons sitting on the ladder.

In the Suzuki-Trotter formula[7] with the finite Trotter number  $N_t$ ,

$$Z \simeq \sum_{\alpha_1} \sum_{\alpha_2} \cdots \sum_{\alpha_{N_t}} \langle \alpha_1 | e^{-\beta\mathcal{J}/N_t} | \alpha_2 \rangle \cdots \langle \alpha_{N_t} | e^{-\beta\mathcal{J}/N_t} | \alpha_1 \rangle, \quad (4)$$

where we denote  $\mathcal{H} - \mu\mathcal{N}$  by  $\mathcal{J}$ . We employ a complete set [8]

$$|\alpha\rangle = |S_1, S_2, \dots, S_{N_r}\rangle \quad (5)$$

with sixteen states in Table I to denote the state  $S_i$  on the  $i$ -th rung, which are the eigenstates for

$$j_i \equiv -\frac{t_r}{2} \sum_{\sigma} [c_{i,a,\sigma}^{\dagger} c_{i,b,\sigma} + h.c.] + \frac{V_r}{2} \sum_{\sigma,\sigma'} n_{i,a,\sigma} n_{i,b,\sigma'} + \frac{U}{2} \sum_l n_{i,l,\uparrow} n_{i,l,\downarrow} - \frac{\mu}{2} \sum_{\sigma,\sigma'} \sum_l n_{i,l,\sigma} n_{i,l,\sigma'}, \quad (6)$$

so that the checkerboard decomposition is available for  $\mathcal{J} = \mathcal{J}_1 + \mathcal{J}_2$ ,

$$\begin{aligned} \mathcal{J}_1 &\equiv -t_c \sum_{\sigma} \sum_l \sum_{k=1}^{N_r/2} [c_{2k-1,l,\sigma}^{\dagger} c_{2k,l,\sigma} + h.c.] + V_c \sum_{\sigma,\sigma'} \sum_l \sum_{k=1}^{N_r/2} n_{2k-1,l,\sigma} n_{2k,l,\sigma'} + \sum_{i=1}^{N_r} j_i, \\ \mathcal{J}_2 &\equiv -t_c \sum_{\sigma} \sum_l \sum_{k=1}^{N_r/2-1} [c_{2k,l,\sigma}^{\dagger} c_{2k+1,l,\sigma} + h.c.] + V_c \sum_{\sigma,\sigma'} \sum_l \sum_{k=1}^{N_r/2-1} n_{2k,l,\sigma} n_{2k+1,l,\sigma'} \\ &\quad + \sum_{i=1}^{N_r} j_i, \quad (7) \end{aligned}$$

where an even  $N_r$  is assumed. Parameters  $u_1$  and  $u_2$  in Table I are given by

$$u_1 \equiv \frac{1}{2} \sqrt{1 + \frac{U}{\sqrt{U^2 + 16t_r^2}}}, \quad u_2 \equiv \frac{1}{2} \sqrt{1 - \frac{U}{\sqrt{U^2 + 16t_r^2}}}.$$

### §3 Numerical results

Now let us show our quantum Monte Carlo results on the model described in the previous section. Here we concentrate our attention on particular values of parameters in the Hamiltonian (1),  $t_c = 1$ ,  $t_r = 2$ ,  $V_c = 2$ ,  $V_r = -4$  and  $U = 4$ . For this choice it is possible to obtain statistically meaningful results while the sign problem is quite serious for other choices we tried.

Because of the emergence of negative weights, we should measure a physical quantity  $A$  in each thermally equilibrated configuration together with its sign and obtain its expectation value by

$$\langle A \rangle_{\text{av}} = \frac{A_{\text{net}}}{Z_{\text{net}}} = \frac{A_+ - A_-}{Z_+ - Z_-}, \quad (8)$$

where  $Z_+(Z_-)$  is the number of configurations with positive (negative) weight, and  $A_+(A_-)$  denotes the contribution from positively (negatively) signed configurations. The  $r$  ratio defined by

$$r \equiv \frac{Z_+ - Z_-}{Z_+ + Z_-}, \quad (9)$$

will inform us how serious the cancellation is.

Changing the number of rungs  $N_r$  ( $8 \leq N_r \leq 32$ ), the inverse temperature  $\beta$  ( $3.3 \leq \beta \leq 10$ ) and the chemical potential  $\mu$ , we measure the doping parameter

$$\delta \equiv 1 - \frac{N_e}{N_s}, \quad (10)$$

where  $N_e \equiv \langle \mathcal{N} \rangle_{\text{av}}$  is the number of electrons and  $N_s \equiv 2N_r$  the number of sites on the ladder, and the charge susceptibility per site,

$$\chi_c \equiv \frac{1}{N_s} \frac{\partial N_e}{\partial \mu} = \frac{\beta}{N_s} (\langle \mathcal{N}^2 \rangle_{\text{av}} - \langle \mathcal{N} \rangle_{\text{av}}^2). \quad (11)$$

Typically we generate 80000 configurations in one measurement by the local update and the global update in the Trotter direction, details of which are in [9], and last 60000 configurations are used for the measurement. Each datum is an average of six such measurements with different random number sequences and the statistical error of the datum is calculated from the standard deviation among these six runs. As we observed very little discrepancy between the  $N_t = 32$  results and the  $N_t = 64$  ones we fixed  $N_t=64$  throughout the measurements. The  $r$ -ratio in the simulations varies from 0.17 to 0.78, depending on values of  $N_r$ ,  $\mu$  and  $\beta$ .

Figure 1 presents the doping parameter  $\delta$  on  $N_s = 16$  (namely  $N_r = 8$ ) and  $N_s = 64$  ladders at  $\beta = 10$  as a function of the chemical potential  $\mu$ . We observe rapid increases of  $\delta$  around  $\mu \sim -1$ , where the system is under the hole doping, and  $\mu \sim 5$  which belongs to the region of the electron doping, together with three plateaus in between. Comparing the results for  $N_s = 16$  and  $N_s = 64$  ladders, we conclude that these plateaus would be split due to the finite size effect and would merge to form the  $\delta = 0$  plateau in the thermodynamic limit, implying a large charge gap  $\Delta_c \sim 6$ . It seems that  $\delta$  changes smoothly in the neighborhood of the half-filling.

Let us then present the data on  $\chi_c$ , the charge susceptibility per site, in more detail. Figure 2(a) plots  $\chi_c$  per site versus  $\delta$  at  $\beta = 10$  on up to an  $N_s = 64$  ladder, choosing several values of  $\mu$  with which we observe two outstanding enhancements of  $\chi_c$  corresponding to the results in Fig. 1. It is notable that for each value of  $\mu$  in the negative  $\delta$  region the values of  $\chi_c$  and  $\delta$  strongly depend on the size of the ladder, while the data for positive  $\delta$  are much less size-dependent except for the value of  $\chi_c$  around  $\delta \sim 0.2$ . In both the positive and the negative  $\delta$  regions the thermodynamic limit of the peak value of  $\chi_c$  for each value of  $\beta$ , which we denote by  $\chi_c^m$ , is successfully obtained by the linear extrapolation of the data  $1/\chi_c$  at the peak for each ladder size versus  $1/N_s$  with  $N_s = 16, 24, 32, 48$  and  $64$ . In Fig. 2(b) we plot these extrapolated values as a function of the temperature  $T \equiv 1/\beta$ . (Note that the ordinate measures the inverse of  $\chi_c^m$ .) Linearly fitted lines to the data drawn in the figure suggests that  $1/\chi_c^m$  reduces to zero (namely  $\chi_c^m$  goes to infinity) near  $T = 0$  in both regions of  $\delta$ . Figure 2(c) shows the values of  $\delta$  to maximize  $\chi_c$  evaluated from the data in Fig. 2(a), which we denote by  $\delta_0$ , as a function of the  $1/N_s$  at temperatures  $T = 0.1, 0.2$  and  $0.3$ . Because of large uncertainties compared to those on the  $\chi_c$  at peaks it is difficult to estimate reliable critical value  $\delta_c$  at which the charge susceptibility diverges, but it is intriguing to note the data suggest finite critical values  $\delta_c \sim 0.2$  and  $\delta_c \sim -0.2$ .

## §4 Discussions

In the previous section we showed our quantum Monte Carlo results on the extended Hubbard ladder model described in §2. What we measure in the simulation are the quantities related to the particle density, the doping parameter  $\delta$  and the charge susceptibility per site  $\chi_c$ , which could signal the charge gap and the phase separation. We find two regions where  $\chi_c$  is greatly enhanced, one of which corresponds to the electron doping ( $\delta < 0$ ) and the other to the hole doping ( $\delta > 0$ ). Linear extrapolations on these enhancements suggest that  $\chi_c$  diverges for the dopings away from the half-filling at the temperatures which are consistent with zero. Between these singularities we observe three plateaus which would merge to one in

the thermodynamic limit to indicate the existence of the large charge gap.

We observe no sign for the singularity of  $\chi_c$  near  $\delta = 0$ , which is in marked contrast to the observations in the one- and two-dimensional standard Hubbard cases where  $\chi_c$  behaves like  $1/\delta$  when  $\delta \sim 0$ [6, 10]. Since it seems difficult to understand our results in the same manner as the latter cases, this feature, together with the enhancement of  $\chi_c$  at finite values of  $\delta$ , implies that a new picture is necessary to explain the behaviors of our model. We would like to stress that this is not quite surprising because studies of the spin 1/2 ladder systems, which corresponds to the  $U \rightarrow \infty$  limit of the half-filled Hubbard models on a ladder, present a picture that differs much from those for the spin 1/2 models on a chain or on a plane[1, 2].

What happens to the model in these regions with the increasing  $\chi_c$  around the non-zero  $\delta_c$  then? Although it is an open question so far and much more work would be necessary to answer it, one clue might be found in the behavior of the double-occupancy-pairs on rungs in the positive  $\delta$  region as well as the vacancy-pairs on rungs in the negative  $\delta$  region.

Let us comment on the hole doping case first. Here we examined the number of doubly occupied sites  $N_d$  and the number of double-occupancy-pairs on rungs  $N_{dd}$  defined by

$$N_d \equiv \langle \mathcal{N}_d \rangle_{\text{av}}, \quad \mathcal{N}_d \equiv \sum_{l=a,b} \sum_{i=1}^{N_r} n_{i,l,\uparrow} n_{i,l,\downarrow} \quad (12)$$

$$N_{dd} \equiv \langle \mathcal{N}_{dd} \rangle_{\text{av}}, \quad \mathcal{N}_{dd} \equiv \sum_{i=1}^{N_r} n_{i,a,\uparrow} n_{i,a,\downarrow} n_{i,b,\uparrow} n_{i,b,\downarrow}, \quad (13)$$

respectively. In the measurement of these quantities for the hole-doped  $N_s = 64$  ladders at  $\beta = 10$ , we observe that the ratio of doubly occupied sites to all sites,  $N_d/N_s$ , linearly increases from 0 to  $\sim 0.4$  as  $\delta$  decreases from  $\sim 0.5$  to  $\sim 0$ . Comparing this ratio with the number of double-occupancy-pairs on rungs divided by the number of rungs,  $N_{dd}/N_r$ , we see that most of these doubly occupied sites prefer pairing on rungs. In order to clarify contributions of the double-occupancy-pairs on rungs to the charge susceptibility  $\chi_c$ , we then divide  $\chi_c$  into three parts  $P_1$ ,  $P_2$  and  $P_3$  and measured them separately. Here we let  $P_1$  represent the portion which

is proportional to the susceptibility concerning to the double-occupancy-pairs on rungs,  $\chi_{dd}$ ,

$$P_1 \equiv \frac{\beta}{N_s} (\langle 4\mathcal{N}_{dd}^2 \rangle_{\text{av}} - \langle 4\mathcal{N}_{dd} \rangle_{\text{av}}^2) = \beta \times 8\chi_{dd}, \quad (14)$$

$$\chi_{dd} \equiv \frac{1}{N_r} (\langle \mathcal{N}_{dd}^2 \rangle_{\text{av}} - \langle \mathcal{N}_{dd} \rangle_{\text{av}}^2), \quad (15)$$

$P_2$  the portion concerning to other states,

$$P_2 \equiv \frac{\beta}{N_s} (\langle \mathcal{N}_{oth}^2 \rangle_{\text{av}} - \langle \mathcal{N}_{oth} \rangle_{\text{av}}^2), \quad \mathcal{N}_{oth} \equiv \mathcal{N} - 4\mathcal{N}_{dd}, \quad (16)$$

and  $P_3$  the interference term

$$P_3 \equiv 2\frac{\beta}{N_s} (\langle \mathcal{N}_{dd}\mathcal{N}_{oth} \rangle_{\text{av}} - \langle \mathcal{N}_{dd} \rangle_{\text{av}} \langle \mathcal{N}_{oth} \rangle_{\text{av}}).$$

Figure 3 shows results for  $P_1$  and  $P_2$  on an  $N_s = 64$  ladder with  $\beta = 10$  together with  $\chi_c$  as a function of the chemical potential  $\mu$ . We clearly see that the double-occupancy-pairs on rungs have dominant effects in the rapid increase of  $\chi_c$ .

In the case of the electron doping we turn our attention to the number of the vacant sites,  $N_v$ , calculated by

$$N_v = N_s - N_d - (N_e - 2N_d) = N_s\delta + N_d, \quad (17)$$

the number of the vacancy-pairs on rungs,  $N_{vv}$ , and the susceptibility concerning to these pairs,  $\chi_{vv}$ , which are defined using  $h_{i,l,\sigma} \equiv 1 - n_{i,l,\sigma}$  instead of  $n_{i,l,\sigma}$  in eqs.(13) and (15). We observe approximately particle-hole symmetric behaviors of  $N_v$  and  $N_{vv}$  for  $-0.5 < \delta < -0.1$  in comparison with the hole doping case. We also observe that the susceptibility  $\chi_{vv}$  shows a remarkable enhancement which suggests that the vacancy-pairs play an important role when  $\chi_c$  diverges in the region  $\delta \sim -0.3$ , although the relation between  $\chi_{vv}$  and  $\chi_c$  is more complicated than that between  $\chi_{dd}$  and  $\chi_c$ .

Several remarks on the future work are in order. Correlation functions corresponding to the susceptibilities  $\chi_c$ ,  $\chi_{dd}$  and  $\chi_{vv}$  would be worth studying to understand whether the long-range order exists in this model. It will be important to measure the magnetic susceptibility and the specific heat in order to shed the light



on the physics of the model. As was mentioned in §2, we had to limit ourselves to a particular choice of parameters  $t_c$ ,  $t_r$ ,  $V_c$ ,  $V_r$  and  $U$  in the simulation because of the sign problem. It would be a future task to study this model for other values of the parameters. It would be also interesting to investigate such an extended model in a bilayer system whose planes are the two-dimensional counterparts of the chains in the ladder system, where the realistic choice of parameters might be realized.

## References

- [1] E. Dagotto and T. M. Rice: Science **271** (1996) 618.
- [2] K. Hida: J.Phys. Soc. Jpn. **60** (1991) 1347.  
T. Barnes, E. Dagotto, J. Riera and E. S. Swanson: Phys. Rev. **B47** (1993) 3196.  
H. Watanabe: Phys. Rev. **B50** (1994) 13442.  
Y. Nishiyama, N. Hatano and M. Suzuki: J. Phys. Soc. Jpn. **64** (1995) 1967.
- [3] E. Dagotto, J. Riera and D. Scalapino: Phys. Rev. **B45** (1992) 5744.  
H. Tsunetsugu, M. Troyer and T. M. Rice: Phys. Rev. **B49** (1994) 16078; Phys. Rev. **B51** (1995) 16456.
- [4] R. M. Noack, S. R. White and D. J. Scalapino: Phys. Rev. Lett. **73** (1994) 182; Europhys. Lett. **30** (1995) 163.  
K. Yamaji and Y. Shimoi: Physica **C222** (1994) 349.  
Y. Asai: Phys. Rev. **B52** (1995) 10390.  
K. Kuroki, T. Kimura and H. Aoki: preprint cond-mat/9610038.
- [5] G. G. N. Angilella, R. Pucci and F. Siringo: Phys. Rev. **B54** (1996) 15471.  
E. V. L. de Mello: Physica **C259** (1996) 109.  
J. van den Brink, R. Eder and G. A. Sawatzky: preprint cond-mat/9704004.  
H. Seo and H. Fukuyama: preprint cond-mat/9704038.
- [6] N. Kawakami and A. Okiji: Phys. Rev. **B40** (1989) 7066.  
A. Moreo, E. Dagotto and D. Scalapino: Phys. Rev. **B43** (1991) 11442.  
N. Furukawa and M. Imada: J. Phys. Soc. Jpn. **61** (1992) 3331.
- [7] M. Suzuki: Prog. Theor. Phys. **56** (1976) 1454; J. Stat. Phys. **43** (1986) 883.  
M. Makivić: *Computational Approaches in condensed-matter physics*, ed. S. Miyashita, M. Imada and H. Takayama (Springer-Verlag, Berlin, 1992) p.129.
- [8] T. Munehisa and Y. Munehisa: Phys. Rev. **B49** (1994) 3347; Prog. Theor. Phys. **92** (1994) 309.

[9] T. Munehisa and Y. Munehisa: Prog. Theor. Phys. **93** (1995) 251.

[10] M. Imada: BUTSURI **48** (1993) 437 (Japanese).

## Figure Captions

### Figure 1

Monte Carlo results on the doping parameter  $\delta$  as a function of the chemical potential  $\mu$  measured on  $N_s = 16$  and  $N_s = 64$  ladders at the inverse temperature  $\beta = 10$ . All the statistical errors are within symbols.

### Figure 2

(a) The charge susceptibility per site,  $\chi_c$ , versus the doping parameter  $\delta$  measured for the chemical potential ranging  $-1.35 \leq \mu \leq -0.95$  and  $5.0 \leq \mu \leq 5.3$  on the  $N_s = 16, 24, 32, 48$  and  $64$  ladders at  $\beta = 10$ . All the statistical errors for  $\delta$  are within symbols. The statistical errors for  $\chi_c$  are within symbols if not shown explicitly.

(b) Temperature dependence of the inverse peak value of the charge susceptibility per site extrapolated to  $N_s \rightarrow \infty$ , which we denote by  $1/\chi_c^m$ . Squares (circles) are symbols for the data with negative (positive)  $\delta$ . Errors evaluated in the process of the extrapolation are within symbols. The result from the linear fit for the data with negative (positive)  $\delta$  is also shown in the figure with a solid (dotted) line.

(c) Values of  $\delta_0$ , the values of  $\delta$  to maximize  $\chi_c$ , at  $T = 0.1, 0.2$  and  $0.3$  as a function of  $1/N_s$ . We evaluate  $\delta_0$  by the peak among the measured data in Fig. 2(a) and estimate its errors by the difference of the two values of  $\delta$  around the peak.

### Figure 3

Contributions of the double-occupancy-pairs on rungs and other states to the charge susceptibility  $\chi_c$  measured in the positive  $\delta$  region on an  $N_s = 64$  ladder at the inverse temperature  $\beta = 10$ , as a function of the chemical potential  $\mu$ . Open circles, open squares and filled circles represent  $P_1$ ,  $P_2$  and  $\chi_c$  defined by eqs. (14),(16) and (11), respectively. Statistical errors are within symbols.

## Table Captions

**Table I**

States on two sites of the  $i$ -th rung used to construct a complete set in the Suzuki-Trotter formula.  $|00\rangle$  represents a state with no electron on either site of the rung.

| $No.$ | state  |
|-------|--|
| 1     | $ 00\rangle$   |
| 2     | $\frac{1}{\sqrt{2}}(c_{i,a,\uparrow}^\dagger + c_{i,b,\uparrow}^\dagger)  00\rangle$   |
| 3     | $\frac{1}{\sqrt{2}}(c_{i,a,\uparrow}^\dagger - c_{i,b,\uparrow}^\dagger)  00\rangle$   |
| 4     | $\frac{1}{\sqrt{2}}(c_{i,a,\downarrow}^\dagger + c_{i,b,\downarrow}^\dagger)  00\rangle$   |
| 5     | $\frac{1}{\sqrt{2}}(c_{i,a,\downarrow}^\dagger - c_{i,b,\downarrow}^\dagger)  00\rangle$   |
| 6     | $c_{i,a,\uparrow}^\dagger c_{i,b,\uparrow}^\dagger  00\rangle$   |
| 7     | $\frac{1}{\sqrt{2}}(c_{i,a,\uparrow}^\dagger c_{i,b,\downarrow}^\dagger + c_{i,a,\downarrow}^\dagger c_{i,b,\uparrow}^\dagger)  00\rangle$   |
| 8     | $\frac{1}{\sqrt{2}}(c_{i,a,\uparrow}^\dagger c_{i,a,\downarrow}^\dagger - c_{i,b,\uparrow}^\dagger c_{i,b,\downarrow}^\dagger)  00\rangle$   |
| 9     | $[u_1(c_{i,a,\uparrow}^\dagger c_{i,b,\downarrow}^\dagger - c_{i,a,\downarrow}^\dagger c_{i,b,\uparrow}^\dagger) + u_2(c_{i,a,\uparrow}^\dagger c_{i,a,\downarrow}^\dagger + c_{i,b,\uparrow}^\dagger c_{i,b,\downarrow}^\dagger)]  00\rangle$ |
| 10    | $[u_2(c_{i,a,\uparrow}^\dagger c_{i,b,\downarrow}^\dagger - c_{i,a,\downarrow}^\dagger c_{i,b,\uparrow}^\dagger) - u_1(c_{i,a,\uparrow}^\dagger c_{i,a,\downarrow}^\dagger + c_{i,b,\uparrow}^\dagger c_{i,b,\downarrow}^\dagger)]  00\rangle$ |
| 11    | $c_{i,a,\downarrow}^\dagger c_{i,b,\downarrow}^\dagger  00\rangle$   |
| 12    | $\frac{1}{\sqrt{2}}(c_{i,a,\uparrow}^\dagger c_{i,a,\downarrow}^\dagger c_{i,b,\uparrow}^\dagger + c_{i,a,\uparrow}^\dagger c_{i,b,\uparrow}^\dagger c_{i,b,\downarrow}^\dagger)  00\rangle$   |
| 13    | $\frac{1}{\sqrt{2}}(c_{i,a,\uparrow}^\dagger c_{i,a,\downarrow}^\dagger c_{i,b,\uparrow}^\dagger - c_{i,a,\uparrow}^\dagger c_{i,b,\uparrow}^\dagger c_{i,b,\downarrow}^\dagger)  00\rangle$   |
| 14    | $\frac{1}{\sqrt{2}}(c_{i,a,\uparrow}^\dagger c_{i,a,\downarrow}^\dagger c_{i,b,\downarrow}^\dagger + c_{i,a,\downarrow}^\dagger c_{i,b,\uparrow}^\dagger c_{i,b,\downarrow}^\dagger)  00\rangle$   |
| 15    | $\frac{1}{\sqrt{2}}(c_{i,a,\uparrow}^\dagger c_{i,a,\downarrow}^\dagger c_{i,b,\downarrow}^\dagger - c_{i,a,\downarrow}^\dagger c_{i,b,\uparrow}^\dagger c_{i,b,\downarrow}^\dagger)  00\rangle$   |
| 16    | $c_{i,a,\uparrow}^\dagger c_{i,a,\downarrow}^\dagger c_{i,b,\uparrow}^\dagger c_{i,b,\downarrow}^\dagger  00\rangle$   |

Table I

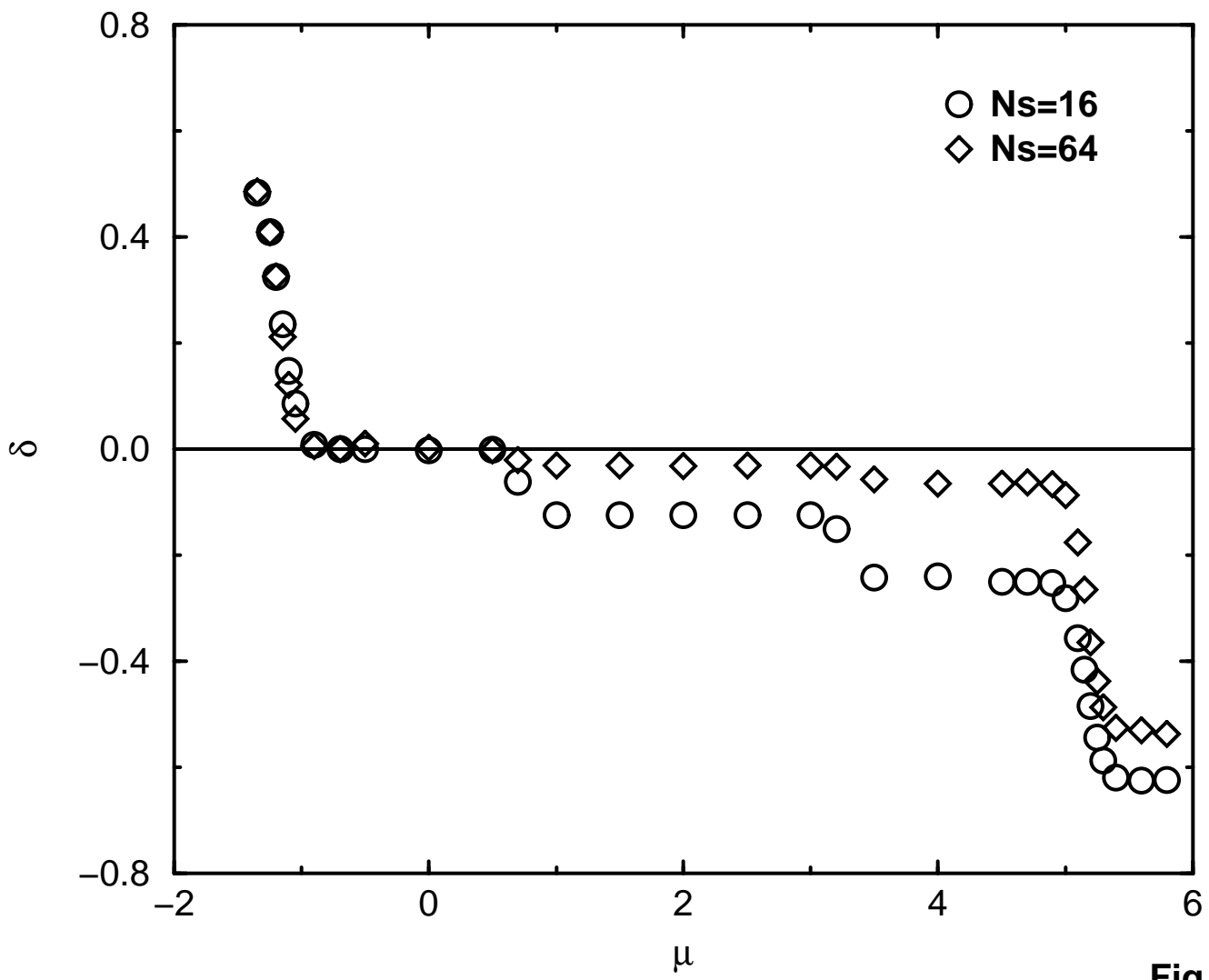


Fig.1

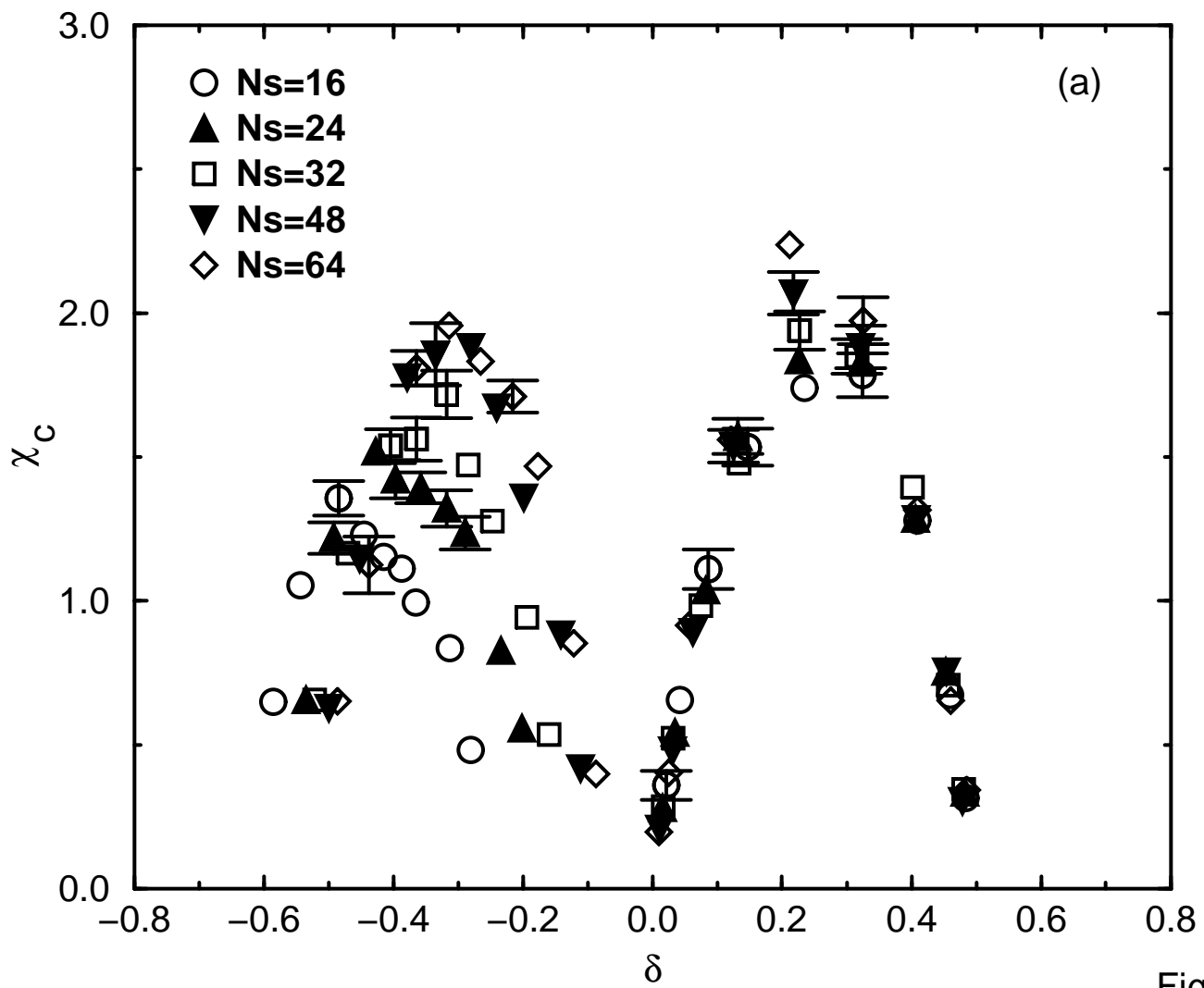


Fig.2

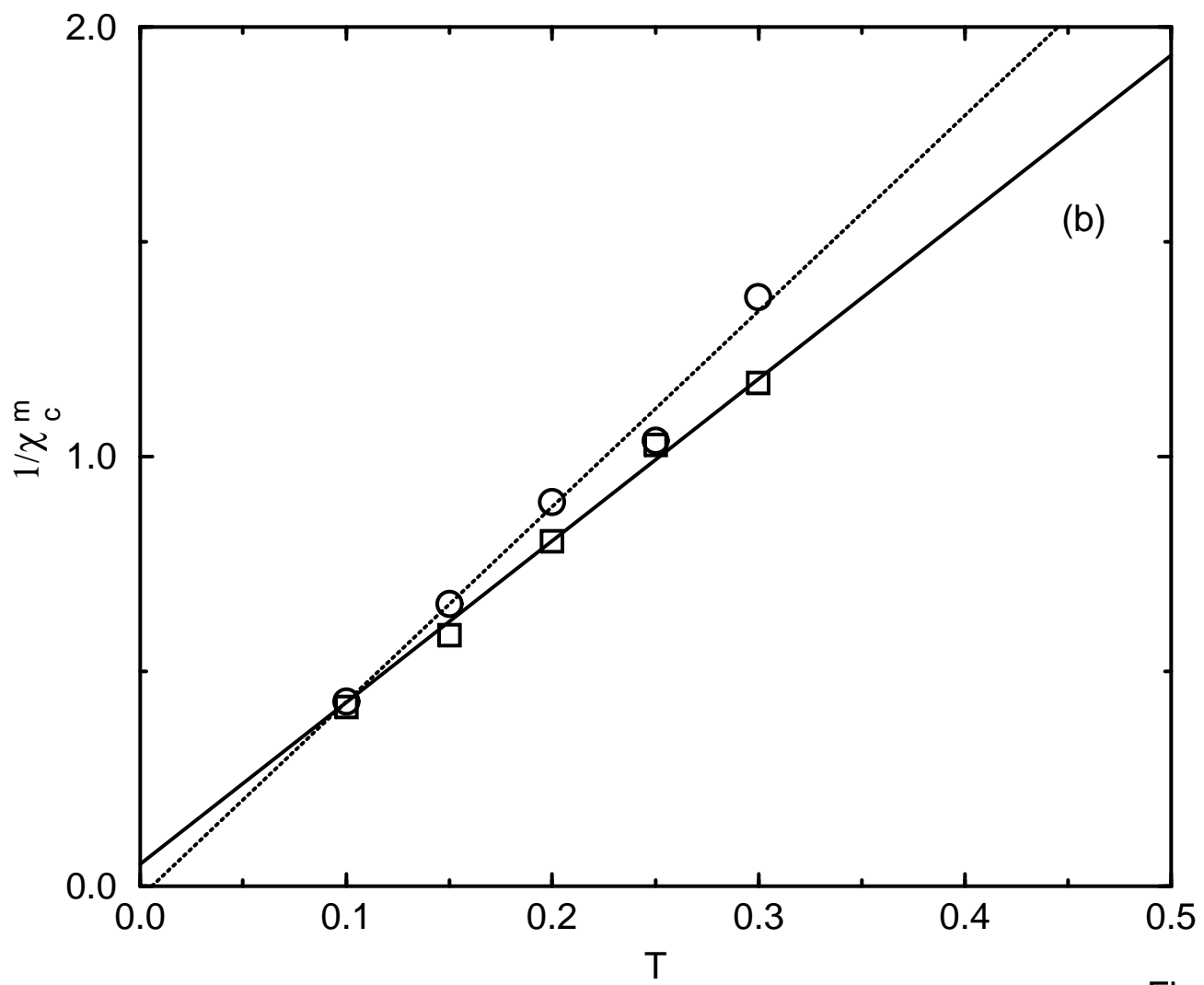


Fig.2

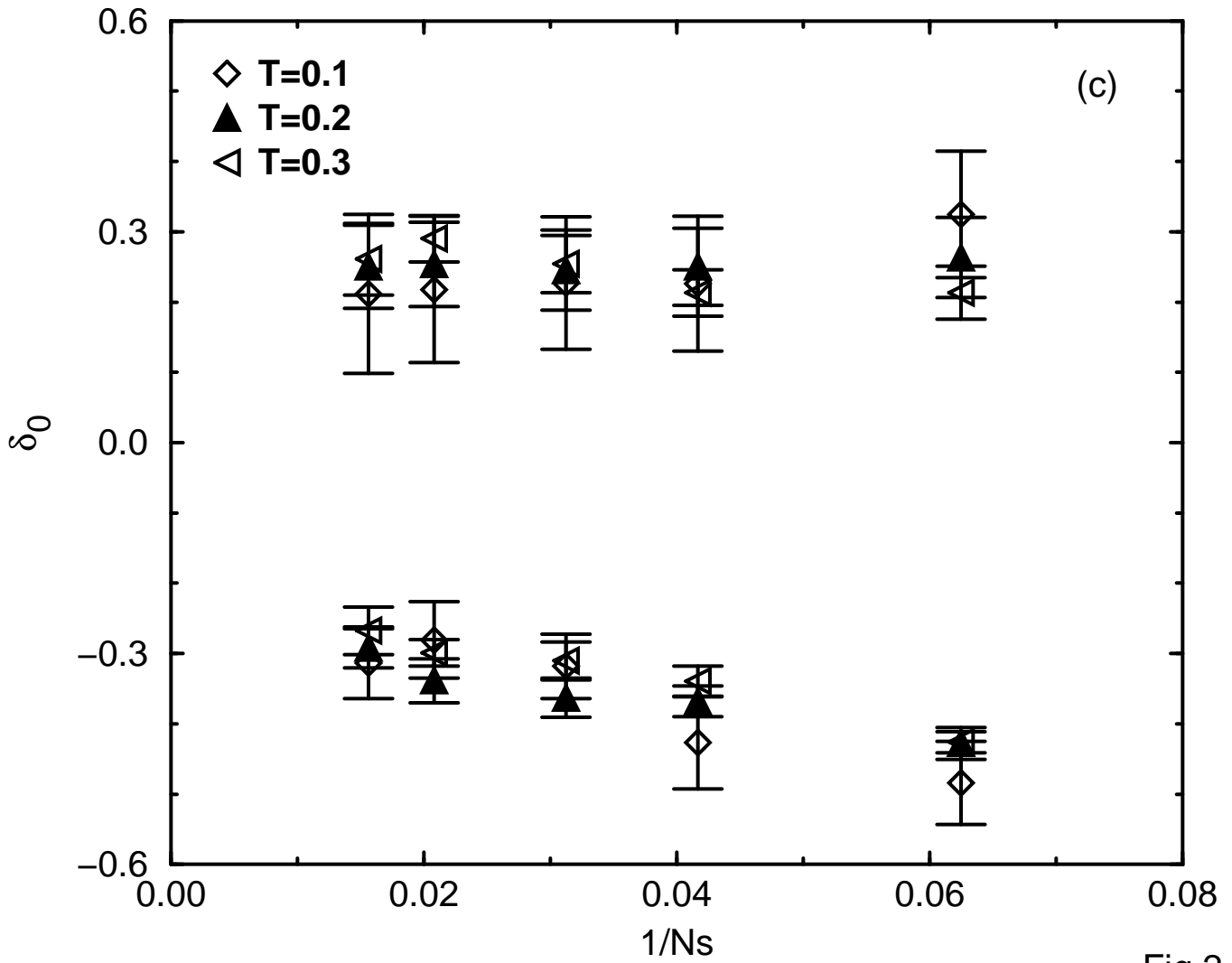


Fig.2



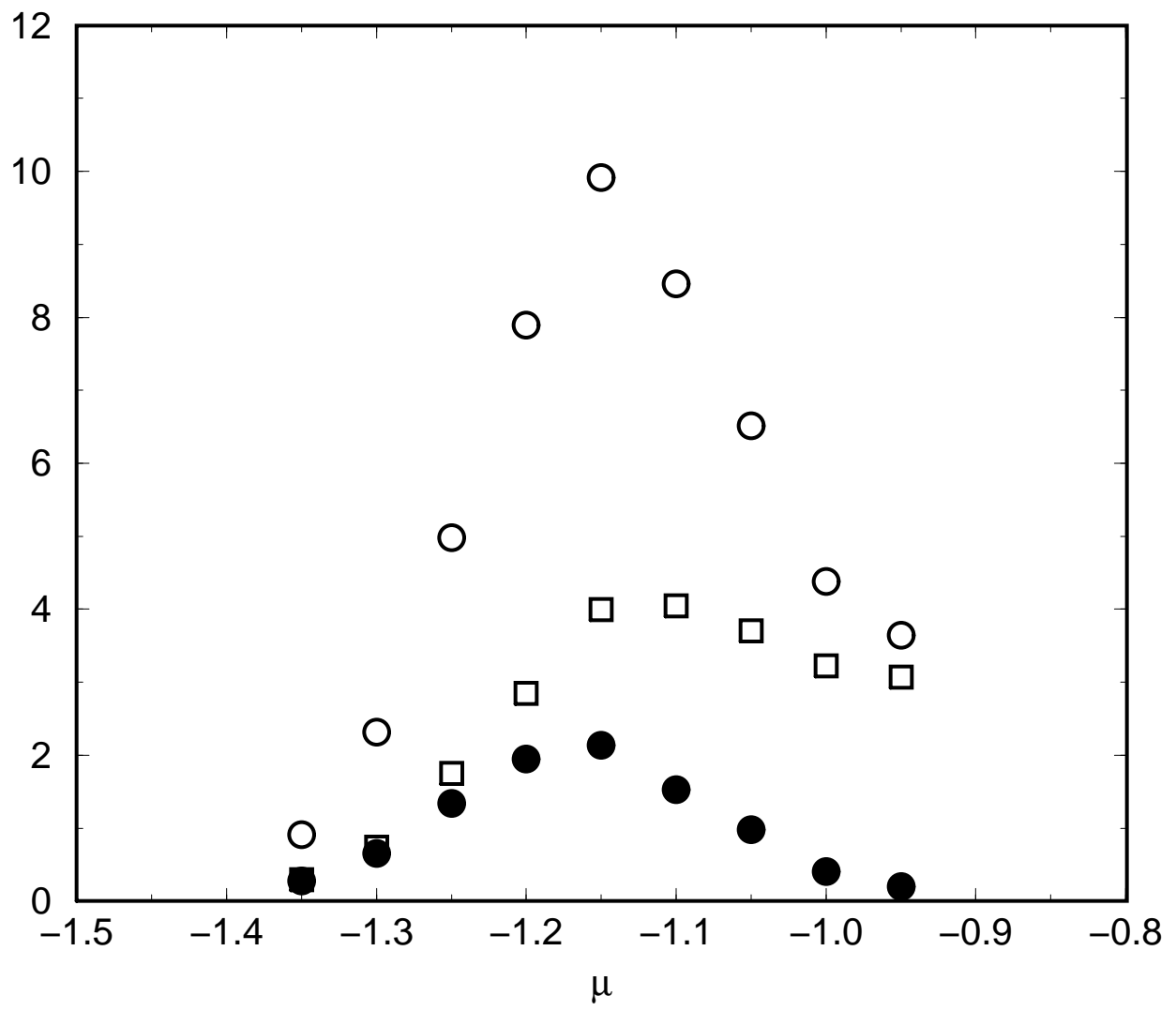


Fig.3